Thermodynamically consistent fluid particle modelling of phase separating mixtures

Thieulot, Cedric

CHAPTER 5

Diffusion in a binary mixture

A previously formulated smoothed particle hydrodynamics model for a phase separating mixture is tested for the case when viscous processes are negligible and only mass and energy diffusive processes take place. We restrict ourselves to the case of a binary mixture that can exhibit liquid-liquid phase separation. The thermodynamic consistency of the model is assessed and the potential of the model to study complex pattern formation in the presence of various thermal boundaries is illustrated.

This chapter has been submitted for publication as : SPH *model for phase separating fluid mixtures. II Diffusion in a binary mixture*, C. Thieulot, P.Español and L.P.B.M. Janssen, to Phys. Rev. E.

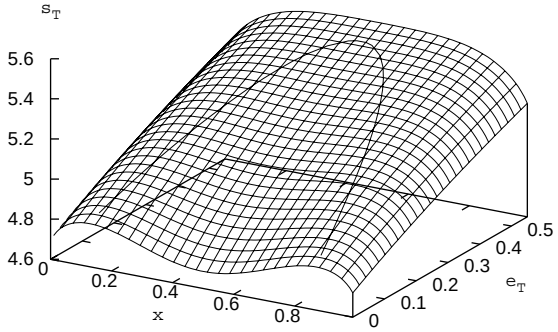

Figure 5.1: 3-dimensional plot of the molecular entropy $s_T = S_T/N_0$ of the system as a function of the concentration x and the molecular energy $e_T = E_T/N_0$. The solid line on the surface is the coexistence curve.

5.2.2 The transport coefficients

In chapter 3 we presented Green-Kubo expressions for the diffusion transport coefficients in the form

$$D_i^{\alpha\beta} = \frac{1}{2k_B T_i}\frac{1}{\mathcal{V}_i}\int_{-\infty}^{\infty} dt \frac{1}{3}\langle \mathbf{V}^\alpha \cdot \mathbf{V}^\beta(t)\rangle_i^{\mathrm{eq}}, \tag{5.22}$$

where T_i is the temperature, $\mathcal{V}_i$ is the volume of the fluid particle and the average velocity of species α is defined as

$$\mathbf{V}^\alpha = \sum_{i_\alpha}^{N^\alpha} \mathbf{v}_{i_\alpha}, \tag{5.23}$$

where $\mathbf{v}_{i_\alpha}$ is the velocity of the i-th molecule of species α within the i-th fluid particle. The equilibrium average $\langle\cdots\rangle_i^{\mathrm{eq}}$ is one of molecular nature, that is to say, with an ensemble which is microcanonical in the total energy and total momentum of the fluid particle. The total momentum of the fluid particle is zero in this equilibrium ensemble. As a consequence, restrictions (5.1) apply because if we multiply $D_i^{\alpha\beta}$ by m_α and sum over species we get inside the equilibrium average the term $\sum_\alpha m_\alpha \sum_{i_\alpha}^{N^\alpha} \mathbf{v}_{i_\alpha}$ which is the total momentum of the system. Because the equilibrium average is microcanonical in the momentum with zero momentum, the average vanishes, leading to (5.1). In a binary mixture, we only have to consider a single diffusion coefficient. Starting with D^{AA}, we present an estimate of this diffusion coefficient based on the overall amplitude of the velocity correlation at time $t = 0$. At this initial time, it is possible to compute the

equilibrium average with the result

$$\frac{1}{3}\langle \mathbf{V}^A \cdot \mathbf{V}^A \rangle_i^{\mathrm{eq}} = N_i^A \frac{k_B T_i}{m^A}. \tag{5.24}$$

Therefore we have $D_i^{AA} = \frac{n_i^A}{m_A}\tau(n_i^A, n_i^B, T_i)$ where $n_i^\alpha = N_i^\alpha/\mathcal{V}_i$. In addition to this we have introduced the correlation time of the velocity

$$\tau^A(n_i^A, n_i^B, T_i) = \frac{1}{2}\int_{-\infty}^{\infty} dt \frac{\langle \mathbf{V}^A \cdot \mathbf{V}^A(t) \rangle_i^{\mathrm{eq}}}{\langle \mathbf{V}^A \cdot \mathbf{V}^A \rangle_i^{\mathrm{eq}}}. \tag{5.25}$$

This is the correlation time of the average velocity of species A. In principle, this correlation time depends on the thermodynamic state of the fluid particle. We would like to have a simple model for this correlation time as a function of the state of the fluid particle. Note that the restriction (5.1) implies the following relationship between τ^A and τ^B

$$m_A n_i^A \tau^A(n_i^A, n_i^B, T_i) = m_B n_i^B \tau^B(n_i^A, n_i^B, T_i). \tag{5.26}$$

This equation clearly shows that $\tau^A(n_i^A, n_i^B, T_i)$ and $\tau^B(n_i^A, n_i^B, T_i)$ must depend on n^A, n^B, otherwise (5.26) cannot generally be fulfilled. The simplest possible assumption would then be to take $\tau^A = n^B m_B c$ and $\tau^B = n^A m_A c$, where c is a constant, independent of the thermodynamic state. Therefore, we will assume the following model for the diffusion coefficient

$$\begin{aligned} D^{AA} &= n^A n^B \frac{m_B}{m_A} c, \\ D^{BB} &= n^A n^B \frac{m_A}{m_B} c, \end{aligned} \tag{5.27}$$

or, in terms of the variables N_0, x and for the simple case that the molecules have the same mass $m_A = m_B$,

$$D^{AA} = D^{BB} = n_0^2 x(1-x)c. \tag{5.28}$$

The corresponding transport coefficient D_i introduced in (5.2) and appearing in the dynamic equations (5.4), (5.5) will take the form of

$$D_i = D_0 x_i(1-x_i), \tag{5.29}$$

where $D_0 = m_0^2 n_0 c$ is a constant. Note that the diffusion-like transport coefficient vanishes in the limits of simple A, B fluids, where $x = 1, 0$.

Although a simple argument like the one presented above for the diffusion-like coefficient D_i is not easily available for the cross-coefficient S_i, we assume that the functional form of S_i is also of the form

$$S_i = S_0 x_i(1-x_i), \tag{5.30}$$

where S_0 is also a constant.

5.3 The equilibrium state

The dynamic equations (5.4) and (5.5) conserve the total energy, the total number of molecules of species A and the total mass of every fluid particle $m_0 N_0$. In addition, they ensure that the total entropy is a monotonously increasing function of time. As a consequence, the dynamic equations (5.4) and (5.5) have a final equilibrium state $x^{\rm eq}$ that maximises the total entropy subject to the conservation of the energy and the number of molecules of species A. In terms of the dynamic variable x_i, the total number of molecules of species A is $N_0^A(x) = N_0 m_0 \sum_i x_i$. In order to obtain the equilibrium state, we maximise without any restriction the following function

$$S(x) - \frac{1}{T_0}(E(x) - \mu_0 N_0^A(x)), \tag{5.31}$$

where T_0 and μ_0 are suitable Lagrange multipliers. The maximum of the function (5.31) occurs at the equilibrium value $x^{\rm eq}$ which, in principle, will be a function of T_0, μ_0. The actual values of T_0, μ_0 are obtained by requiring that $x^{\rm eq}(T_0, \mu_0)$ fulfils the constraints

$$\begin{aligned} \sum_i U_i &= E_0, \\ N_0 \sum_i x_i &= N_0^A, \end{aligned} \tag{5.32}$$

where E_0 is the total energy of the system and N_0^A is the total number of molecules of species A in the system. Note that in Eq. (5.32) we assumed that there are no surface tension terms in the energy, just for the sake of simplicity. The maximisation of the function (5.31) leads to the following set of equations, one for each fluid particle

$$\begin{aligned} \frac{\partial S}{\partial U_i} &= \frac{1}{T_0}, \\ \frac{\partial S}{\partial x_i} &= \frac{\mu_0}{T_0}. \end{aligned} \tag{5.33}$$

We can rewrite these equations simply by using the definitions (5.21) for the intensive parameters:

$$\begin{aligned} T(x_i^{\rm eq}, U_i^{\rm eq}) &= T_0, \\ \mu(x_i^{\rm eq}, U_i^{\rm eq}) &= \mu_0, \end{aligned} \tag{5.34}$$

The above equations simply state that the equilibrium state is such that all the fluid particles have the same temperature and chemical potential. The solution of the coupled set of equations (4.79) provides the equilibrium state $U_i^{\rm eq}, x_i^{\rm eq}$ of Eqs. (5.4) and (5.5) that is reached as time tends towards infinity. On the other hand, the chemical potential $\mu(x)$ is defined as being the difference between μ^A and μ^B (see chapter 4) and we know that the chemical potentials for each component in a mixture tend towards a unique value at

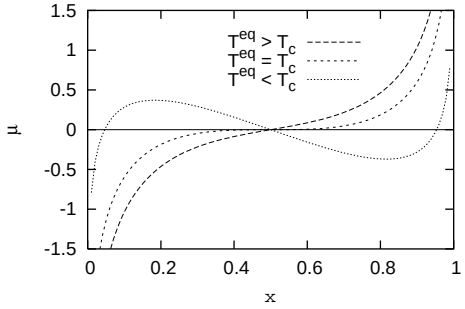

Figure 5.2: Representation of the chemical potential μ as a function of the concentration for different temperatures.

equilibrium [24], leading us to expect $\mu(x_i^{\rm eq}, U_i^{\rm eq}) = 0$. By considering Eq. (5.21), the equilibrium value of the concentration x_i^{eq} is the solution of the equation

$$k_B T^{eq} \ln \frac{1 - x_i^{\rm eq}}{x_i^{\rm eq}} + 2n_0 \mathtt{a}\Lambda(2x_i^{eq} - 1) = 0, \tag{5.35}$$

where we have assumed $a_{AA} = a_{BB}$, this is $\zeta = 0$ for the sake of simplicity. The curve $T^{eq} = f(x_i^{eq})$ is the coexistence curve. The critical point is defined by the coordinates

$$x_i = \frac{1}{2}, \quad T_c = \frac{\Lambda a n_0}{k_B}, \tag{5.36}$$

above which constituents A and B form a homogeneous solution regardless of their concentration.

On Fig. 5.2 the chemical potential in Eq. (5.21) is plotted for different values of the ratio T^{eq}/T_c. If $T^{eq} > T_c$ we observe that the equation $\mu(x_i^{\rm eq}, U_i^{\rm eq}) = 0$ has a unique solution $x = 1/2$. If on the other hand $T^{eq} < T_c$, then two additional solutions appear, symmetrical with respect to $x = 1/2$. Due to the dependence of T_c on Λ, it is obvious that this is only valid if $\Lambda > 1$, which means that when molecules of equal type attract each other with greater force than those of unequal type, phase separation may occur.

5.4 Simulation set up

We perform numerical simulations of the dynamic equations (5.4) and (5.5). N_T fluid particles are arranged in a regular two dimensional lattice with periodic boundary conditions. In this way, the volume of every fluid particle is exactly the same. The first order differential equations are integrated with a fourth-order Runge-Kutta algorithm. Every fluid particle interacts with their neighbors according to the range h of the weight function $W(r)$. We select as the weight function the Lucy function defined by

$$W(r) = \frac{5}{\pi h^2}\left(1 + 3\frac{r}{h}\right)\left(1 - \frac{r}{h}\right)^3. \tag{5.37}$$

which is normalised to unity in 2D [25].

We recall in what follows the large set of parameters that enter into the model and make suitable selections in order to limit the scope of this very rich model. The first set of parameters are of molecular nature and appear in the equations of state. These are the mass of the molecules, m_α, the excluded volumes of both species b_α, the attraction parameters $a_{\alpha\beta}$, and the parameters $c_{\alpha\beta}$ controlling surface tension. In order to keep the number of parameters to a minimum, we assume that the mass of the molecules of both species is the same, *i.e.* $m_A = m_B = m_0$. Also, the excluded volume of both species is assumed to be equal, $b_A = b_B = b$ as well as the attraction parameters $a_{AA} = a_{BB} = a$. This means that the parameters defined in Eq. (5.8) become

$$\Lambda = 1 - \frac{a_{AB}}{a}, \qquad \zeta = 0. \tag{5.38}$$

In this paper, we will limit ourselves to the case $\Lambda = 1$ which means that there is absolutely no attraction between molecules of different species. Although physically unlikely, we expect this to favor phase separation when it is expected to occur.

The second set of parameters corresponds to the global parameters of the simulation. These include the size L of the periodic cubic box, the total mass of the system M_T, the total energy of the system E_T, and the number density x of molecules of species A. These global parameters fix the final thermodynamic state of the system. The next set of parameters correspond to the transport coefficients D_0, S_0 appearing in Eqs. (5.29), (5.30). We assume that the thermal conductivity κ is a constant, independent of the state of the fluid particles. Finally, we have a set of algorithm dependent parameters: h, the radius of the support of the weight function $W(r)$, the number N_T of fluid particles and the integration time step.

There are many other important parameters in the simulation, but they are all derived from the above parameters. We can further reduce the number of independent parameters by choosing a set of four basic units. In this article we are considering the following "molecular units": the unit of length is $L_u = b^{1/D}$ the linear dimension of a molecule, the unit of mass is $M_u = m_0$, the mass of a molecule, the unit of entropy is $S_u = k_B$, the Boltzmann constant, and the unit of temperature is $T_u = T_c$ the critical temperature of the liquid-liquid phase transition. The units of the rest of the variables are trivially obtained from the aforementioned. For instance, the unit of energy will be $E_u = k_B T_c$. We shall further denote dimensionless quantities by the use of starred variables (*).

The input parameters in a simulation run are taken to be the overall number density n_0, the total mass fraction x of species A and the dimensionless box size $L^\star = L/b^{1/D}$. The range of possible values are $n_0 \in]0, 1[$ and $x \in [0, 1]$, otherwise the entropy function and equations of state are ill-defined.

The total number of molecules in the system is given in terms of these input parameters as $N_{\text{mic}} = n_0 V^\star$, the total number of A molecules as $N_T^A = x N_{\text{mic}}$, and B molecules as $N_T^B = (1 - x) N_{\text{mic}}$, whereas the total dimensionless mass is $M^\star = M_T/m_0 = N_{\text{mic}}$. The next input parameter is N_T, which is the total number of fluid particles. From this we can compute the typical interparticle distance $\lambda^\star = L^\star/N_T^{1/D}$, the mass of a fluid

	E1	E2	E3	E4	E5	E6	E7	E8	E9
N_T	4096	1024	4096	16384	4096	4096	4096	4096	4096
Λ	1	1	1	1	1	1	1	1	1
n_0	0.3	0.3	0.3	0.3	0.3	0.3	0.3	0.3	0.3
$L^\star$	360	180	360	720	360	360	360	360	360
$T^\star_{init}$	1.1	0.6	0.6	0.6	0.7	0.9	0.95	0.8	0.75
x	0.5	0.5	0.5	0.5	0.5	0.5	0.5	0.35	0.7

Table 5.1: Parameters of simulations E1-E9.

particle $m = M_T/N_T$ or in dimensionless units $m^\star = N_{\rm mic}/N_T$, and the total number of molecules per fluid particle $N_0 = N_{\rm mic}/N_T$. In addition the overlapping coefficient $s = h/\lambda$ is also an input that allows us to compute the dimensionless range of the weight function as $h^\star = sL^\star/N_T^{1/D}$. The chosen value is $s = 2.5$ since it insures that the difference between the volume of the box and the sum of all the cell volumes obtained through SPH theory is very small. The definition of the critical temperature in Eq. (5.36) implies that the dimensionless attraction parameter $a^\star = a/(bk_BT_c)$ is fixed to the value $a^\star = 1/(\Lambda n_0^\star)$.

While the Soret-like coefficient S_0 is set to zero for simplicity, the diffusion coefficient and the thermal conductivity coefficient values reflect those of Argon, and we also use the atomic mass and atomic size of Argon in order to obtain dimensionless values of the used parameters.

In order to solve our set of first order differential equations, we have to provide a set of initial conditions for the state variables. For the concentration $x_i(t = 0)$ we assign the input concentration x to a particle plus a random contribution within a range of $\pm 0.2\%$ of x, while still keeping $\langle x_i \rangle = x$. This destabilises slightly the initial state and insures that the system is not set at an artificial computational equilibrium. On the other hand, all temperatures are assigned to T_{init}. The value of T_{init} fixes the global energy content of the system.

5.5 Simulation results

Nine simulations, whose input parameters are listed in table 5.5, were carried out until the system reached equilibrium. For instance, E1 is a simulation of $N_{\rm mic} = n_0V^\star = n_0(L^\star)^D = 38880$ molecules, such that each fluid particle contains $N_0 = N_{\rm mic}/N_T \simeq 9.5$ molecules.

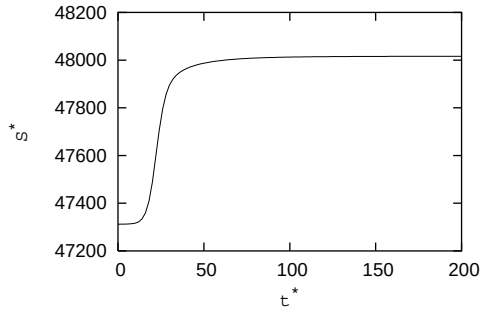

Figure 5.3: Total entropy $S^\star$ given by Eq.(5.13) as a function of time.

5.5.1 Equilibrium phase diagram

Without surface tension

Simulations are conducted first in the absence of the surface tension terms, i.e. all $\tilde{\tilde{\phi}}$-related terms are set to zero. In every simulation, we observe that the total entropy is an strictly increasing function of time, until the equilibrium state is achieved (Fig. 5.3). As expected, the entropy increases until it reaches a plateau, therefore complying with the second law of thermodynamics for isolated systems, while the total energy is conserved to machine precision.

For under-critical situations we expect the values of $\{x_i\}_{\text{eq}}$ to fall into two sets, one which consists of A-rich fluid particles and another, of B-rich particles. This is indeed what happens: the original distribution of concentrations artificially centered on $x = 1/2$ at $t = 0$, evolves towards a two-peak distribution, as can be seen on Fig. 5.4.

When the system is completely phase-separated, we can define two quantities: $x_d < 0.5$, the average concentration of *dark* (B-rich) particles and $x_l > 0.5$ the average concentration of *light* (A-rich) particles. When N_T takes high values, the number of A-rich and B-rich particles are equal, leading to $x_d = 1 - x_l$. It is important to note that although theory would predict two Dirac peaks, the outcome of our simulation consist of two very narrow distributions due to the finite number of particles and to the finite simulation time.

One of the observations of these simulations without surface tension, is that neighboring fluid particles can have A or B rich phases independent of the state of the given fluid particle. In the simulations, an alternating pattern of A and B rich fluid particles arises. The size of the domains of A rich regions is essentially that of a fluid particle, see Fig. 5.5.

It is also important to remember that although fully phase-separated, the system tends towards a unique equilibrium pressure, a unique equilibrium temperature, and a unique value (equal to zero) of the chemical potential, which was verified in all the conducted experiments.

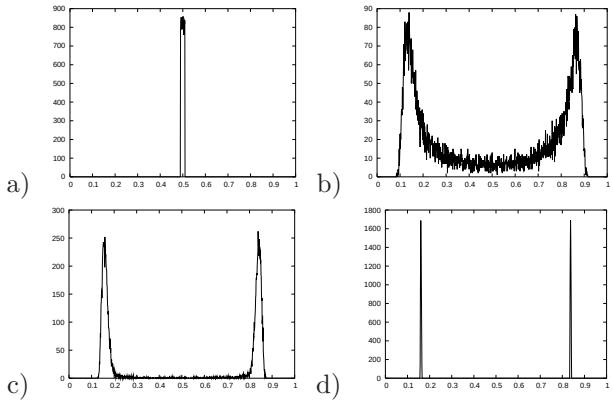

Figure 5.4: Concentration distribution of the particles for E_4at t=0 (a), t=100 (b), t=350 (c) and t=1000 (d). Time in dimensionless units.

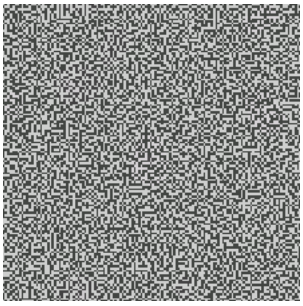

Figure 5.5: Phase separated fluid mixture of E_4: the 2-dimensional box is divided in 64×64 particles that either become A- or B- rich. The composition of a cell in species A is indicated in gray scale.

	E10	E11
N_T	1024	1024
Λ	1	1
n_0	0.3	0.3
$L^\star$	180	180
$T^\star_{init}$	1.1-1.225	0.6-0.78
x	0.075-0.925	0.075-0.925
$E^\star_T/N_{\rm mic}$	0.6	0.1

Table 5.2: Parameters of simulations E10 and E11.

A very stringent test for the thermodynamic consistency of the model is that the numerical value of the total entropy function evaluated at the equilibrium state $S(x^{\rm eq}) = \sum_i S(N_0, \{x_i\}_{\rm eq}, \{U_i\}_{\rm eq})$ is equal to the entropy function Eq. (5.19) (which describes the thermodynamic behavior of a fluid particle) evaluated at the global system values of $N_{\rm mic}, x, E_T$. In this way, even though we only specify the thermodynamic behavior of the fluid particles, the full system behaves in a similar thermodynamic way.

We have run two simulations E10 and E11 which differ in the overall energy of the system, as shown in table 5.5.1. Simulation E10 is above the critical point and one sees on Fig. 5.6 that we have a very good agreement between the equilibrium value of the total entropy of the system and the entropy function in Eq. (5.14) of a fluid particle evaluated at the value of the extensive variables of the whole system.

On the other hand the simulation E11 is clearly subcritical and one observes on Fig. 5.6 that the simulation points tend to follow a straight line between the two expected peaks. This can be explained in the following way: at equilibrium the fully phase separated system presents $x_d N_T$ B-rich particles and $(1-x_d)N_T$ A-rich particles, all of them at the same equilibrium temperature, and therefore all having the same internal energy (see Eq.(5.21)), leading to write

$$\begin{aligned} S^\star_T &= \sum_i S^\star(x_i, U^\star_i) \\ &= x_d N_T S^\star(x_d, U^\star) + (1-x_d) N_T S^\star((1-x_d), U^\star) \\ &= N_T S^\star(x_d, U^\star). \end{aligned}$$

The total entropy of the system therefore stays constant regardless of the overall concentration of the system. On the other hand, if the overall concentration x is outside the interval $[x_d, x_l]$, the system does not phase separate and the total entropy of the system follows the theoretical curve, as can be seen on Fig. 5.6.

Last, we have compared the theoretical and simulated coexistence curves. From Eq. (5.21), while using the units defined above, one can write the chemical potential as follows ($\Lambda = 1$, $\zeta = 0$):

$$\mu^\star_i = -T^\star_i \ln \frac{1-x_i}{x_i} - 2(2x_i - 1), \tag{5.39}$$

and the coexistence curve in the T, x space is then given by

$$T_i^\star = \frac{2(2x_i - 1)}{\ln \frac{x_i}{1-x_i}}. \tag{5.40}$$

In Fig 5.7 we plot the equilibrium temperature $T^{eq} < 1$ as a function of the concentrations x_d and x_l for the simulations $\text{E}_{2,\ldots 9}$. We also perform another simulation, E_{12}, that shares its parameters with E_3, but we vary the initial temperature from 0.35 until 0.999. We indeed observe that our code converges towards the expected values of x_d and x_l. In all cases the agreement between theory and simulation results is excellent. It is interesting to remark that E_2, E_3 and E_4 are very similar in the sense that N_0 (the number of molecules per particle) is the same for all, but the size of E_4 is a system 4 times bigger than E_3 itself 4 times bigger than E_2, leading to the conclusion that the size of the sample for a given physical experiment is irrelevant regarding the outcome of the simulations.

We plot also in Fig. 5.7 the spinodal curve which is the metastability limit of the binary mixture. The mixture becomes unstable inside the spinodal (leading to full phase separation) while it is metastable between the coexistence and the spinodal curves. Its locus is given by the change of sign of the curvature of the entropy, i.e. where $\partial\mu/\partial x_i^{eq} = 0$ at constant energy. When simulations were initially started in between the two curves phase separation occurred or not depending on the randomness on the initial values of x_i.

With surface tension included

When we introduce the surface tension terms, there is an energy cost for having neighbor particles with (too) different concentrations. The system now segregates into regions of A and B rich mass fraction separated by smooth interfaces. In Fig. 5.8 we compare the distribution of mass fraction for the simulation E_3 with and without the surface tension terms. The two equilibrium values of the mass fraction have not changed appreciably, but the width of the distribution is larger when surface tension is included. The width of the distribution of mass fraction is a reflection of the smooth transition occurring in the interfacial regions. It is quite remarkable that the introduction of surface tension does not change the phase diagram (i.e. the location of the peaks in Fig. 5.8). However for this to happen, it is necessary that the size of the interfacial region separating A and B regions is small compared with the total size of the system. Because the interface width grows as we approach the critical point, system size dependences are observed near the critical point.

We explore the effect of the magnitude of the surface tension effects by setting a coefficient q in front of every surface tension term in the equations (i.e. the $\tilde{\phi}$ terms), and look at the system for different values of $q \in [0:1]$. We run a simulation with 256x256 particles, with $T_{init} = 0.6$ for a time t=300 dimensionless time units. The system does not reach the equilibrium state in this time. In Fig. 5.9 we present the distribution of mass fraction for 5 values of q, while in Fig. 5.10 snapshots of the system at this time are

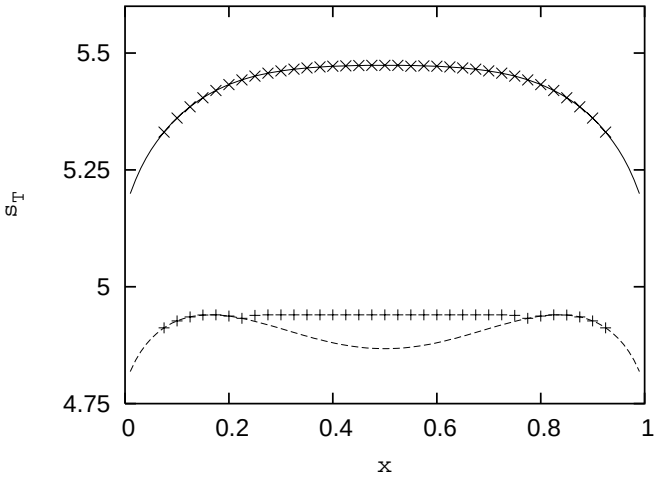

Figure 5.6: Equilibrium value of the total entropy per molecule $s_T = S_T/N_{mic}$ of the system as a function of x for $e_T = E_T/N_{mic} = 0.6$ (plain) with its corresponding simulation results ($\times$) and for $e_T = E_T/N_{mic} = 0.1$ (dashed) with its corresponding results ($+$).

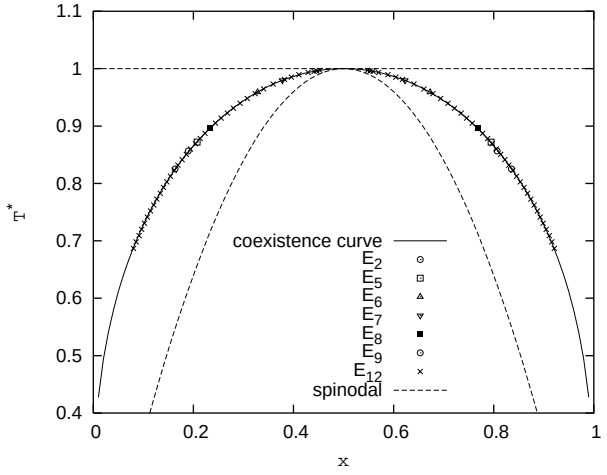

Figure 5.7: The concentrations of the coexisting phases at different temperatures. The solid line stands for the theoretical coexistence curve, while the symbols are results from the numerical simulations.

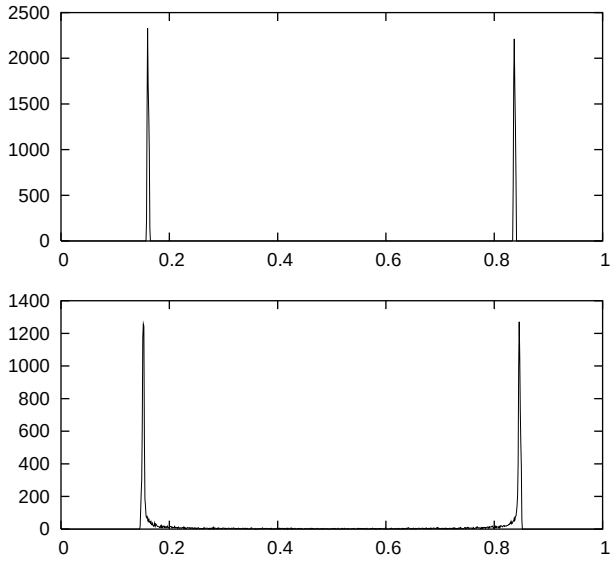

Figure 5.8: Distribution of particles' concentration x_i in the case of no surface tension (above), and in the case where surface tension terms are included (under). Parameters are those of E_3.

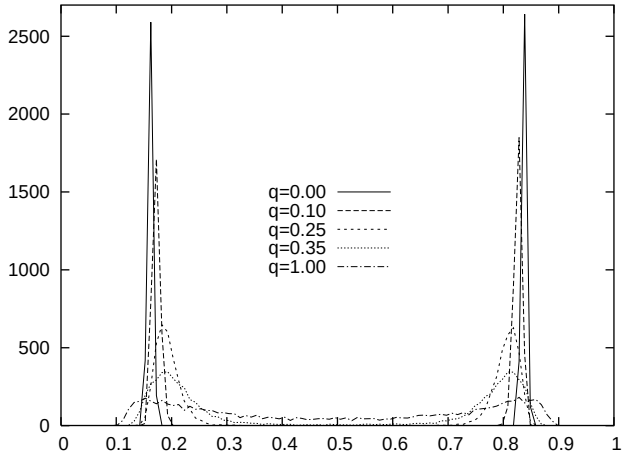

Figure 5.9: Particle distribution at the same time for different values of coefficient q.

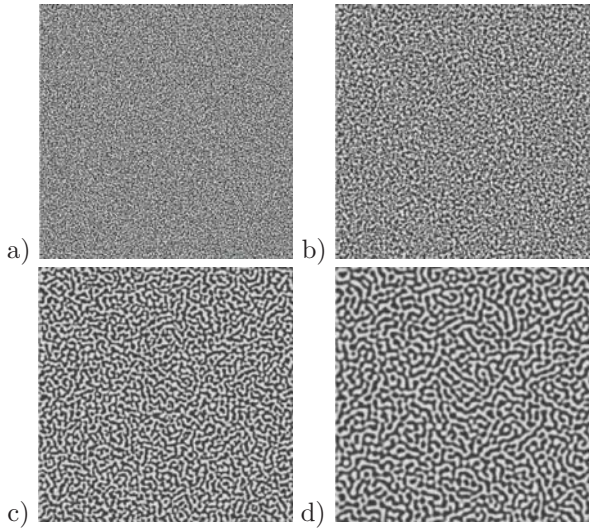

Figure 5.10: Effect of the intensity of the surface tension term on the patterns of spinodal decomposition of otherwise identical samples, $q = 0$ (a), $q = 0.35$ (b), $q = 0.5$ (c), $q = 1$ (d).

presented for different values of q. We observe that the larger the intensity of the surface tension, the wider the peaks of the distribution of mass fraction. This is a reflection that the domains are larger the larger is the intensity of the surface tension and, in addition, the interfacial width is larger the larger is the intensity of the surface tension.

In order to illustrate that the model can tackle more complex and interesting situations, we set our system at an initial upper-critical temperature of 1.3 and impose a gradient of temperature as follows: all particles in the middle horizontal axis are suddenly cooled down to a temperature of 0.5, while all particles at upper horizontal border of the box are maintained at the initial temperature 1.3. This is achieved by means of an extra term in the $\dot{U}_i$ equation:

$$-\kappa_g(T_i^\star - \mathcal{T}_i), \tag{5.41}$$

where κ_g is the heat conductivity of the hypothetical cooling system lying underneath our system, and $\mathcal{T}_i$ is the temperature desired at particle i.

We present in Fig. 5.11 a time sequence of the phase separation under a temperature gradient. The sudden cooling of the central line produces a space and time varying temperature field. The critical isotherms are two horizontal lines that move from the center outwards towards the top and bottom of the system. At the steady state they are located at $y \approx \pm 0.3$. In between these two isotherms the temperature is under-critical and the system phase separates. Initially the domains have a typical length scale characteristic of spinodal decomposition and have no particular orientation. As

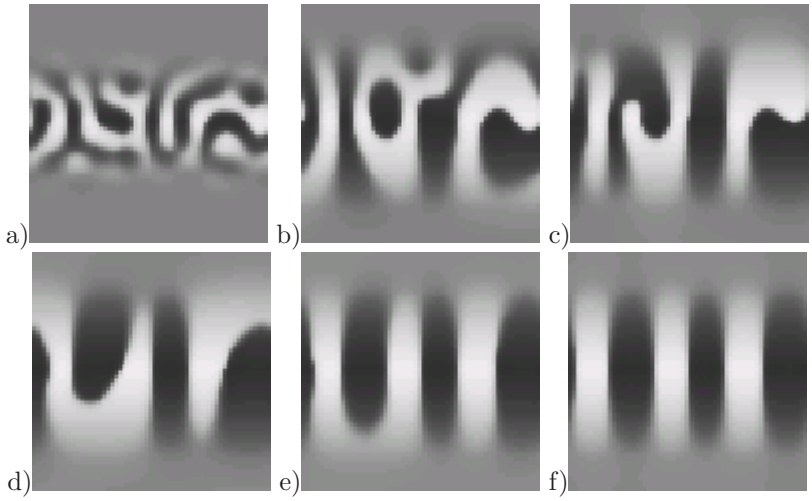

Figure 5.11: Evolution of an upper-critical binary mixture at $T^{\star}_{init} = 1.01$ when two horizontal lines are suddenly brought to temperatures $T^{\star}_{hot} = 1.3$ (in the middle of the sample) and $T^{\star}cold = 0.5$ (at the bottom/top of the sample, which has periodic boundary conditions) thus creating a two-ramp temperature gradient. The different pictures correspond to times a) $t^{\star}$=400, b) $t^{\star}$=3200, c) $t^{\star}$=7400, d) $t^{\star}$=13000, e) $t^{\star}$=19600, f) $t^{\star}$=75000. (x=0.5, N_T=4096, $L^{\star}$=360).

time proceeds, though, the domains align parallel to the temperature gradient with a characteristic length scale. The blurred edges near to the hot bath lines indicate the position of the critical isotherms. Similar simulations of mixtures in the presence of temperature gradients have been reported by Jasnow and Viñals [21]. Note, however that in counter-distinction with the present work, the simulations in Ref. [21] are those on a model in which the temperature is not dynamically coupled to the concentration field.

Another experiment was performed: we set the system at initial temperature 1.01 but set $\mathcal{T}_i = 0.5$ for the particle in the middle of the system by the same means described here above. This would mimic the effect of inserting a cold needle in an upper-critical mixture. It results first in a succession of concentric rings that ultimately evolve towards a unique drop formed in the middle of the system, see Fig. 5.12. The initial mass fraction is $x = 0.5$, but we have also experimented with other concentrations leading to square symmetrical arrangements (due to the periodic boundary conditions) of many droplets of the minority phase. These droplets are expected to merge in an extremely long time scale in a one single droplet.

Note that this interesting and intriguing patterns can have far reaching technological applications. For if the binary mixture phase can be further solidified through rapid quenching, the resulting material properties of the structures can have rather different

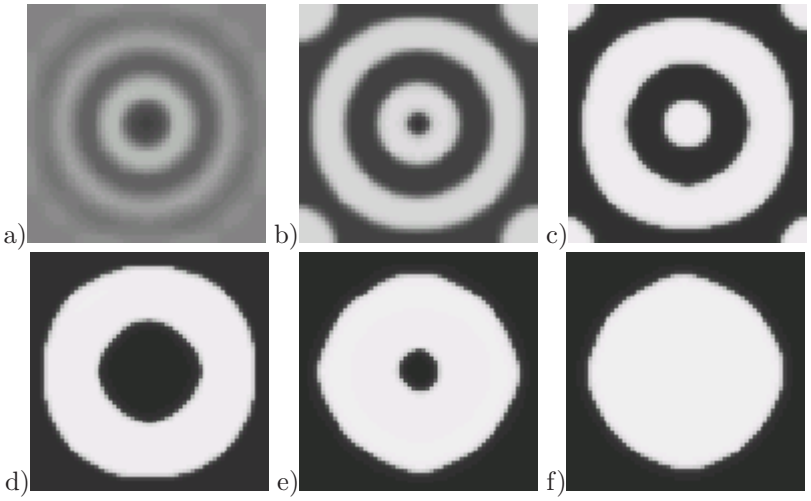

Figure 5.12: Evolution of an upper-critical binary mixture at $T^\star_{init} = 1.01$ when single "needle" at the middle of the sample is maintained at an under-critical temperature $T^\star_{cold} = 0.6$. The different pictures correspond to times a) $t^\star$=2000, b) $t^\star$=10000, c) $t^\star$=30000, d) $t^\star$=60000, e) $t^\star$=200000, f) $t^\star$=300000. (x=0.5, N_T=4096, $L^\star$=360).

mechanical and structural properties, different from the originally mixed systems. The theoretical understanding and control of these patterns in non-isothermal situations can open the way to the construction of techniques for designing new composite polymer materials with valuable properties.

5.6 Discussion

In this paper, we have validated through numerical simulations the SPH model for phase separating mixtures in the simplest non-trivial case. Viscous processes are neglected and only mass and energy diffusive processes take place. We also restricted ourselves to the case of a binary mixture that can exhibit only liquid-liquid phase separation. The model satisfies the First and Second Law of thermodynamics: the total energy of the system is conserved and the total entropy of the system is an increasing function of time. The van der Waals thermodynamic behavior is recovered by the simulations when they reach the equilibrium state. Below the critical temperature the mixture phase separate and regions of A-rich or B-rich regions appear separated by diffuse interfaces. The role of the strength of the surface tension has been qualitatively investigated in the dynamics of the formation of domains. We observe that higher surface tension implies slower dynamics along with larger domains and interface widths. We have observed that near the critical point, when the interfaces are larger, the simulated coexistence curve departs slightly

from the van der Waals prediction. We believe though, that this is a system size effect that disappears when the system size is much larger than the typical interface width of the separated domains.

In this preliminary work, we have investigated qualitatively the effect of imposing non-homogeneous temperature distributions on the dynamics of the phase separation. Temperature inhomogeneities created either by walls at different temperatures or local sinks of energy lead to very interesting pattern formation with a complex dynamics that deserves future investigation.

The discrete fluid particle model that we have presented in this paper allows one to describe liquid-liquid phase transition but not gas-liquid transitions that, in principle, are accommodated by the more general model in chapter 4. The reason is that the number density of every fluid particle is fixed in the simulation. The particles do not move, their volume is fixed and the mass of a fluid particle is constant. We expect that when the particles are allowed to move according to the dynamic equations presented in chapter 3, in the region of thermodynamic parameters where the van der Waals equation of state predicts gas-liquid coexistence, the fluid particles will distribute in space in such a way to produce liquid regions of high density (the fluid particles all have the same mass or N_0, but they are packed together so their volumes are small) coexisting with gas-like sparse distributions of fluid particles. In particular, we expect that for a simple fluid with $x_i = 1$ the model allows one to describe the usual van der Waals gas-liquid transition. Simulations of coexisting liquid droplets with its vapor have been conducted in Ref. [26] with the SPH method. However, surface tension was treated in a rather unconventional way by using a a weight function with different ranges. In counter-distinction to our model where the coefficients $c_{\alpha\beta}$ control surface tension, there is no direct control to the surface tension in the model of Ref. [26]. We plan to address this issue in a future work.

Bibliography

[1] *free energy of nonuniform systems. I-Interfacial free energy*, J.W. Cahn and J.E. Hilliard, J. Chem. Phys. **28**, 258 (1958).

[2] *Spinodal decomposition in binary gases*, S. Bastea and J.L. Lebowitz, Phys. Rev. Lett. **78**, 3499 (1997).

[3] *Binary fluids with long range segregating interaction. I: derivation of kinetic and hydrodynamic equations*, S. Bastea, R. Esposito, J.L. Lebowitz, and R. Marra, J. Stat. Phys. **101**, 1087 (2000).

[4] *A phase field model of capillarity*, L.K. Antanovskii, Phys. Fluids **7**, 747 (1994).

[5] *Quasi-incompressible Cahn-Hilliard fluids and topological transitions*, J. Lowengrub and L. Truskinovsky, Proc. R. Soc. London A **454**, 2617 (1998).

[6] *Diffuse-interface models for two-phase flow*, P. Papatzacos, Physica Scripta **61**, 349 (2000).

[7] *The description of a multicomponent mixture by the density functional method when there are surface phases present*, O. Dinariyev, J. Appl. Maths Mechs. **65**, 471 (2001).

[8] *Diffuse-interface methods in fluid machanics*, D.M. Anderson, G.B. McFadden, and A.A. Wheeler, Annu. Rev. Fluid Mech. **30**,139 (1998).

[9] *Thermodynamics for a van der Waals fluid*, P. Español, J. Chem. Phys. **115**, 5392 (2001).

[10] *Investigation of a two-phase fluid model*, B.T. Nadiga and S. Zaleski, Eur. J. Mech. B/Fluids **15**, 885 (1996).

[11] *Calculation of two-phase Navier-Stokes flows using phase-field modeling*, D. Jacqmin, J. Comp. Phys. **155**, 96 (1999).

[12] *3D spinodal decomposition in the inertial regime*, V.M. Kendon, J.-C. Desplat, P. Bladon and M.E. Cates, Phys. Rev. Lett. **83**, 576 (1999).

[13] *Inertial effect in three-dimensional spinodal decomposition of a symmetric binary fluid mixture: a lattice Boltzmann study*, V.M. Kendon, M.E. Cates, J.-C. Desplat, I. Pagonabarraga, and P. Bladon, J. Fluid Mech. **440**, 147 (2001).

[14] *Computer simulations of domain growth and phase separation in two-dimensional binary immiscible fluids using dissipative particle dynamics*, P.V. Coveney and K.E. Novik, Phys.Rev.E **54**, 5134 (1996).

[15] *Hydrodynamic bubble coarsening in off-critical vapor-liquid phase separation*, P.B. Warren, Phys. Rev. Lett. **87**, 225702-1 (2001).

[16] *Dissipative particle dynamics for interacting systems*,I. Pagonabarraga and D. Frenkel, J. Chem. Phys. **115**, 5015 (2001).

[17] *Phase separation in two-dimensional fluid mixtures*, G. Leptoukh, B. Strickland, and C. Roland, Phys. Rev. Lett. **74**, 3636 (1995).

[18] *Dynamics of phase separation of a simple fluid mixture: comparison between molecular dynamics and numerical integration of the phenomenological equation*, H. Furukawa, Phys. Rev. E **55**, 1150 (1997).

[19] *Phase ordering in fluids*, J.M. Yeomans, Ann. Rev. Comp. Phys. VII, ed. D. Stauffer (1999).

[20] *Spinodal decomposition to a lamellar phase: effects of hydrodynamic flow*, G. Gonnella, E. Orlandini, and J. Yeomans, Phys. Rev. Lett. **78**, 1695 (1997).

[21] *Coarse-grained description of thermo-capillarity flow*, D. Jasnow and J. Viñals, Phys. Fluids **8**, 660 (1996).

[22] *Statistical Mechanics of Phases, Interfaces and Thin Films*, H.T. Davis, (Wiley-VCH, New York, 1996).

[23] *Critical lines and phase equilibria in binary van der Waals mixtures*, P.H. Konynenburg and R.L. Scott, Phil. Trans. Roy. Soc. London **298**, 495 (1980).

[24] *Thermodynamics*, H.B. Callen, John Wiley & sons, New York (1960).

[25] *Smoothed Particle Hydrodynamics*, J.J. Monaghan, Annu. Rev. Astron. Astrophys. **30**, 543 (1992).

[26] *Liquid drops and surface tension with smoothed particle applied mechanics*, S. Nugent and H.A. Posch, Phys. Rev. E **62**, 4968 (2000).